Hindawi
Mathematical Problems in Engineering
Volume 2017, Article ID 3960401, 9 pages
https://doi.org/10.1155/2017/3960401

Research Article

Analytical Study on an Oscillating Buoy Wave Energy Converter Integrated into a Fixed Box-Type Breakwater

Xuanlie Zhao,[1] Dezhi Ning,[1] Chongwei Zhang,[1] Yingyi Liu,[2] and Haigui Kang[1]

[1]*State Key Laboratory of Coastal and Offshore Engineering, Dalian University of Technology, Dalian 116024, China*
[2]*Research Institute for Applied Mechanics, Kyushu University, Kasuga 816-8580, Japan*

Correspondence should be addressed to Dezhi Ning; dzning@dlut.edu.cn

Received 15 December 2016; Revised 15 April 2017; Accepted 3 May 2017; Published 30 May 2017

Academic Editor: Oleg V. Gendelman

An oscillating buoy wave energy converter (WEC) integrated to an existing box-type breakwater is introduced in this study. The buoy is installed on the existing breakwater and designed to be much smaller than the breakwater in scale, aiming to reduce the construction cost of the WEC. The oscillating buoy works as a heave-type WEC in front of the breakwater towards the incident waves. A power take-off (PTO) system is installed on the topside of the breakwater to harvest the kinetic energy (in heave mode) of the floating buoy. The hydrodynamic performance of this system is studied analytically based on linear potential-flow theory. Effects of the geometrical parameters on the reflection and transmission coefficients and the capture width ratio (CWR) of the system are investigated. Results show that the maximum efficiency of the energy extraction can reach 80% or even higher. Compared with the isolated box-type breakwater, the reflection coefficient can be effectively decreased by using this oscillating buoy WEC, with unchanged transmission coefficient. Thus, the possibility of capturing the wave energy with the oscillating buoy WEC integrated into breakwaters is shown.

1. Introduction

Breakwaters are commonly constructed at a distance from the coastline, aiming to reduce coastal erosion or provide safe harborage. At shallow-water deployment sites, it is usually convenient to use bottom-sitting breakwaters such as the rubble mound or vertical wall breakwaters. The breakwater structure works by either absorbing the energy of the waves that hit it or simply reflecting the inshore waves away [1]. Due to simplification in structures, the box-type breakwater is most widely applied. It works by reflecting incident waves in a large extent, so that the leeward transmitted waves can be reduced greatly. The hydrodynamic performance of such breakwater has been systematically studied [1–8].

In recent years, the requirement for renewable energy increases greatly. To decrease the construction cost, some new ideas on integrating the wave energy converter (WEC) into some kind of coastal and offshore structures have been raised (Dal Ferro 2006). For example, Michailides and Angelides [9] proposed a flexible floating breakwater. Each breakwater has several hinged floating modules, through whose relative motion the wave energy can be captured. He and Huang [10] integrated the classical oscillating water column (OWC) WEC into the floating breakwater structure. Through experiments, the possibility of using OWC to mitigate the motion of the breakwater and wave transmission was shown. Chen et al. [11] considered two floating cylinders used as both WECs and floating breakwaters. The performance of the device was investigated numerically. He and Huang [12] arranged an OWC device in front of a vertical wall. Their experimental results showed that OWC structure can be served as a wave absorber for reducing wave reflection from the vertical wall. Ning et al. [13] introduced a buoy-type WEC combined with the pile-restrained floating breakwater. Experimental results showed that good wave attenuation performance and energy-conversion efficiency can be achieved, with appropriate dimensions and power take-off (PTO) damping setting. Overall, designs based on the combination of WECs and breakwaters have evident advantages. For example, the WEC and breakwaters can share the cost to a large proportion;

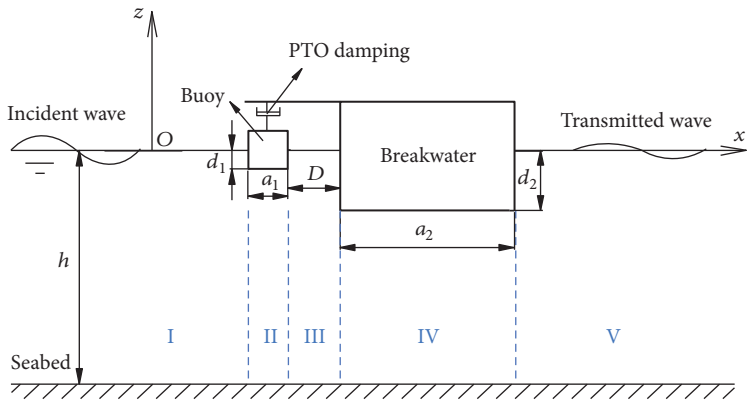

Figure 1: Sketch of the floating structures with a PTO system.

ocean space for WEC device can be saved greatly, and the performance of breakwaters may be further improved.

In this study, we will propose a more economical design by integrating the oscillating buoy WEC into the existing box-type breakwaters. The oscillating buoy WEC works as a floating box in front of the breakwater towards the incident waves. A power take-off (PTO) system is installed on the topside of the breakwater to harvest the kinetic energy of the front buoy. Thus, the energy of incident and reflected waves can be converted to the usable electricity, instead of being reflected away as the typical box-type breakwater does. Theoretically, the buoy in front of the breakwater can capture more wave energy than an isolated oscillating buoy WEC, as a result of the superposition of incident and reflected waves.

At this preliminary design stage, this study will focus on the hydrodynamic performance of this system. Based on the efficiency considerations, the analytical solution of the hydrodynamic problem is firstly derived using potential-flow theory, as in Section 2. Then, in Section 3, validation and parametric studies are conducted, respectively. The reflection coefficient and capture width ratio (CWR) of the system are investigated to show the effectiveness of this device. The wave transmission is also tested to check whether the buoy motion affects the intrinsic performance of the breakwater. In Section 4, the conclusions are drawn.

2. Mathematical Equations

As shown in Figure 1, a floating buoy and a box-type breakwater are placed in the water with uniform depth h. The displacement of the front buoy is much smaller than that of the breakwater. The breadths of two structures are defined as a_1 and a_2, the drafts are d_1 and d_2, respectively, and the spacing in between is D. The mass of the buoy is $M_1 = \rho a_1 d_1$, with ρ as the water density. The buoy can only undergo a heave motion restrained by a spring system. The stiffness coefficient of the spring can be expressed as $K_1 = \rho g a_1$, where g is the gravity acceleration. A 2D Cartesian coordinate system O-xz is defined, whose origin is on the still water plane. The structures are subjected to a train of regular waves travelling in the positive x-direction.

The fluid motion is described by the velocity potential ϕ whose spatial gradient is the fluid velocity. The oscillation system is further assumed to be in a steady state. Then, the velocity potential can be written as

$$\phi(x,z,t) = \mathrm{Re}\left[\Phi(x,z)\, e^{-\mathrm{i}\omega t}\right], \tag{1}$$

where t is the time, $\mathrm{i} = \sqrt{-1}$, ω is the angular frequency, Re denotes the real part of a complex, and Φ is a complex spatial velocity potential. Based on the continuity equation, the following Laplace equation can be obtained:

$$\frac{\partial^2 \Phi}{\partial x^2} + \frac{\partial^2 \Phi}{\partial x^2} = 0. \tag{2}$$

In the linear system, the potential Φ can be further decomposed as

$$\Phi = \Phi_I + \Phi_D + \Phi_{R,1}, \tag{3}$$

where Φ_I is the incident potential, Φ_D is the diffraction potential, and $\Phi_{R,1}$ is the radiation potential due to the heave motion of the buoy. According to the Airy wave theory, the incident potential has the form as follows:

$$\Phi_I = -\frac{\mathrm{i}gA}{\omega} \frac{\cosh k(z+h)}{\cosh kh} e^{\mathrm{i}kx}, \tag{4}$$

where A is the wave amplitude and k is the wavenumber subjected to the dispersion relation $\omega^2 = gk\tanh(kh)$. For the diffraction potential, the governing equation is Laplace equation and the boundary conditions can be written as follows:

$$\begin{aligned}
&\frac{\partial \Phi_D}{\partial z} - \frac{\omega^2}{g}\Phi_D = 0 \\
&\qquad \left(z = 0,\ x < x_{l,1} \text{ or } x_{r,1} < x < x_{l,2} \text{ or } x > x_{r,2}\right) \\
&\qquad\qquad \frac{\partial \Phi_D}{\partial z} = 0 \quad (z = -h) \\
&\frac{\partial \Phi_D}{\partial z} = -\frac{\partial \Phi_I}{\partial z} \quad \left(z = -d_n,\ x_{l,n} < x < x_{r,n},\ n = 1, 2\right) \\
&\frac{\partial \Phi_D}{\partial z} = -\frac{\partial \Phi_I}{\partial z} \\
&\qquad \left(-d_n < z < 0,\ x = x_{r,n} \text{ or } x = x_{l,n},\ n = 1, 2\right) \\
&\qquad \Phi_D \text{ outgoing: finite value}, \quad |x| \longrightarrow \infty.
\end{aligned} \tag{5}$$

Here, $x_{l,n}$ and $x_{r,n}$ denote the x coordinate of the left and right side of pontoon n (pontoon 1 refers to the front buoy and pontoon 2 the breakwater).

As a preliminary study, the rear breakwater is assumed as a fixed structure, which is constrained by vertical piles. The front buoy works in principle of the heave-type oscillating buoy WEC and the kinetic energy in heave mode of the buoy can be converted into the useful energy by using a PTO system. Thus, we can reasonably assume that the front buoy moves in heave mode and the rear pontoon is fixed. For the radiation problem, the buoy is forced to move in heave mode with amplitude $A_{R,1}$ and angular frequency ω. The radiation potential can be expressed as

$$\Phi_{R,1} = -\mathrm{i}\omega A_{R,1}\varphi_{R,1}(x, z), \tag{6}$$

where $A_{R,1}$ is the heave amplitude of the buoy. The function of $\varphi_{R,1}$ also satisfies Laplace equation in the fluid domain. Its boundary conditions can be summarized as

$$\begin{aligned}
&\frac{\partial \varphi_{R,1}}{\partial z} - \frac{\omega^2}{g}\varphi_{R,1} = 0 \\
&\qquad \left(z = 0,\ x < x_{l,1} \text{ or } x_{r,1} < x < x_{l,2} \text{ or } x > x_{r,2}\right) \\
&\qquad\qquad \frac{\partial \varphi_{R,1}}{\partial z} = 0 \quad (z = -h) \\
&\frac{\partial \varphi_{R,1}}{\partial z} = \delta_{m,1} \quad \left(z = -d_m,\ x_{l,m} < x < x_{r,m},\ m = 1, 2\right) \\
&\frac{\partial \varphi_{R,1}}{\partial x} = 0 \\
&\qquad \left(-d_m < z < 0,\ x = x_{r,m} \text{ or } x = x_{l,m},\ m = 1, 2\right) \\
&\qquad \varphi_{R,1} \text{ outgoing: finite value}, \quad |x| \longrightarrow \infty.
\end{aligned} \tag{7}$$

For the solution of the diffraction and radiation potentials, five subdomains I, II, III, IV, and V as indicated in Figure 1 are divided. The detailed expressions of the diffraction and radiation potentials can be found in Zheng and Zhang [14], which is not repeated here.

Then, the motion equation of the buoy can be written as

$$\left(-\omega^2\left(M_1 + \mu_1\right) - \mathrm{i}\omega\left(\lambda_1 + \lambda_{\mathrm{PTO}}\right) + K_1\right)A_{R,1} = F_{z,1}, \tag{8}$$

where λ_{PTO} is the PTO damping imposed on the front buoy. Unless otherwise noted, λ_{PTO} equals the optimal PTO damping ($\lambda_{\mathrm{isolation}}$) of the front buoy in isolation [15, 16]. The added mass μ_1 and radiation damping λ_1 on the buoy in heave motion can be written as

$$\begin{aligned}
\mu_1 &= -\rho \int_{S_1} \mathrm{Re}\left[\varphi_{R,1}\right] n_z \, \mathrm{d}s \\
\lambda_1 &= -\rho\omega \int_{S_1} \mathrm{Im}\left[\varphi_{R,1}\right] n_z \, \mathrm{d}s,
\end{aligned} \tag{9}$$

where Im denotes the imaginary part of a complex. The horizontal force $F_{x,n}$ and vertical force $F_{z,n}$ on pontoon n can be written as

$$\begin{aligned}
F_{x,n} &= -\mathrm{i}\omega\rho \int_{S_n} \left(\Phi_I + \Phi_D\right) n_x \, \mathrm{d}s \\
F_{z,n} &= -\mathrm{i}\omega\rho \int_{S_n} \left(\Phi_I + \Phi_D\right) n_z \, \mathrm{d}s,
\end{aligned} \tag{10}$$

where S_n is the bottom area of the pontoon n ($n = 1, 2$) and n_x and n_z are the unit normal vector along the negative x-axis and negative z-axis.

The CWR as an important efficiency indicator of a WEC is expressed for the front buoy as

$$\eta = \frac{P}{P_{\mathrm{incident}}}, \tag{11}$$

where P is the power produced by the buoy as

$$P = \frac{1}{2}\omega^2 \lambda_{\mathrm{PTO}} \left|A_{R,1}\right|^2. \tag{12}$$

And P_{incident} is the power of incident waves

$$P_{\mathrm{incident}} = \frac{1}{4}\frac{\rho g A^2 \omega}{k}\left(1 + \frac{2hk}{\sinh 2hk}\right). \tag{13}$$

The reflection and transmission coefficients (symbolically, K_R and K_T) can be written as

$$\begin{aligned}
K_R &= \left|\frac{\Phi_D - \mathrm{i}\omega A_{R,1}\varphi_{R,1}}{\Phi_I}\bigg|_{x=-\infty}\right| \\
K_T &= \left|\frac{\Phi_I + \Phi_D - \mathrm{i}\omega A_{R,1}\varphi_{R,1}}{\Phi_I}\bigg|_{x=+\infty}\right|.
\end{aligned} \tag{14}$$

3. Results and Discussions

3.1. Verification. In order to validate the analytical solution, the coefficient of ${K_R}^2 + {K_T}^2 + \eta$ is investigated at different wave conditions. Within the frame of potential-flow theory, the relation of ${K_R}^2 + {K_T}^2 + \eta = 1$ must be satisfied. In this section, we set the geometrical parameters as $a_1 = 1$ m, $a_2 = 6$ m, $d_1 = 1$ m, $d_2 = 2.5$ m, $D = 1$ m, and $h = 10$ m. From Figure 2, it can be seen that the relation of energy conservation is satisfied, which verifies the accuracy of the present analytical model.

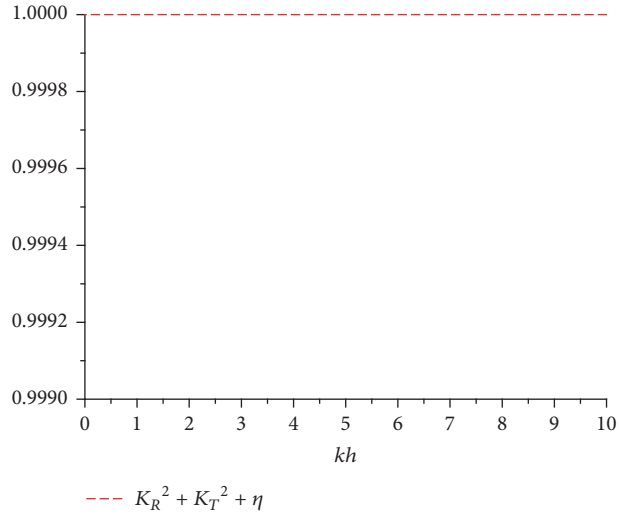

FIGURE 2: Coefficient of $K_R^2 + K_T^2 + \eta$ versus the dimensionless wavenumber kh.

3.2. Effects of Buoy Breadth. Effects of the buoy on the hydrodynamic performance of the breakwater depend on several parameters, that is, the breadth a_1, draft d_1, and spacing D. In addition, the hydrodynamic efficiency of the buoy as the wave energy device is affected by those parameters. Therefore, in the following sections, a parametric study is conducted to investigate the effects of these geometrical parameters.

The effects of the buoy breadth on the reflection coefficient K_R, transmission coefficient K_T, and the CWR η can be found in Figure 3. Four cases with $a_1/h = 0.05$, 0.1, 0.15, and 0.2 (correspondingly, $a_1/a_2 = 1/12$, 1/6, 1/4, and 1/3) are considered. All the other geometrical parameters are kept constant as $a_2/h = 0.6$, $d_1/h = 0.1$, $d_2/h = 0.25$, and $D/h = 0.1$.

Figure 3(a) shows the reflection coefficient of the system. The reflection coefficients of breakwaters with and without the buoy are compared. It is found that the existence of the buoy clearly decreases the wave reflection at a wide range of wavenumbers. For the breakwater with a buoy, two troughs can be found on the curve. One is located in the lower frequency region, while the other is in the higher frequency region. In the lower frequency region, a larger buoy breadth generally leads to a weaker wave reflection. However, at the higher frequency region, the trend is opposite. For each K_R, both troughs gradually shift to lower frequency regions, as the buoy breadth grows.

From Figure 3(b), it is found that the buoy breadth does not affect the transmission coefficient evidently. For the CWR in Figure 3(c), the trend of bimodal curve can be described clearly. As the buoy breadth increases, both the peaks and troughs shift to the lower frequency region. The peak positions and trough positions of the CWR curves actually correspond to those positions in Figure 3(a). The existence of the zero value of CWR (in Figure 3(c)) may be due to the fact that the Bragg resonance with strong reflection occurred at certain frequencies, which led to significant reduction of the extraction efficiency [17]. It is similar for the zero values of CWR that occurred in Figures 4(c) and 5(c). Thus, from the viewpoint of engineering application, the occurrence of these should be avoided by the proper structure design based on the dominated sea states at the deployment site. The peaks in the lower and higher frequency regions increase and decrease with a_1/h increasing, respectively. It is noted that the maximum of CWR of the oscillating buoy with this configuration is obviously greater than that of the isolated one (i.e., 50%) [15].

3.3. Effects of Buoy Draft. Figure 4 further presents effects of the buoy draft on the integrated system. Three cases are considered, by setting the buoy draft as $d_1/h = 0.1$, 0.15, and 0.2 (correspondingly, $d_1/d_2 = 0.4$, 0.6, and 0.8), respectively. The remaining geometrical parameters are kept constant as $d_2/h = 0.25$, $a_1/h = 0.1$, $a_2/h = 0.6$, and $D/h = 0.1$. Similar to Figure 3(a), all curves of reflection coefficients have two troughs. The position of each valley shifts to the lower frequency region, as the buoy draft increases. For the tested cases, as d_1/h decreases, the reflection coefficient has more and more significant reduction in the value close to the trough neighborhood. Moreover, regardless of the variation of buoy draft, the reflection coefficient tends to approach that of an isolated breakwater with the increase of wave frequency. Even so, the reflection coefficient for the breakwater with a buoy is generally smaller than that without front buoy for the considered frequency region. Then consider the transmission coefficient in Figure 4(b). It is found that, except for the large draft case ($d_1/h = 0.2$), the transmission coefficient of the system is not affected much by the buoy draft. For the CWR found in Figure 4(c), two peaks are observed in the curve. The effect of the draft on η is apparently in the opposite trend to that on K_R for $kh > 2$. If we take the frequency region when $\eta > 20\%$ as the effective bandwidth, it can be seen that the effective bandwidth becomes narrower with an increasing d_1/h.

3.4. Effects of Spacing. Effects of the spacing between the buoy and breakwater are further considered in this subsection. The geometrical parameters of two structures are kept constant as $a_1/h = 0.2$, $a_2/h = 0.6$, $d_1/h = 0.1$, and $d_2/h = 0.25$. Figure 5 shows variations of the reflection coefficient K_R, the transmission coefficient K_T, and the CWR η, for different spacing (i.e., $D/h = 0.05$, 0.1, 0.15, and 0.2). The reflection and transmission coefficients corresponding to the breakwater without any buoy are also plotted in the figure for comparison.

Firstly, let us consider the reflection coefficients in Figure 5(a). When the buoy exists, obvious differences of the curves can be found between $kh = 2$ and $kh = 8$. Two troughs can still be seen in each curve. In the lower frequency region, the troughs value of K_R shows an increasing trend as the spacing D/h increases. From Figure 5(b), it is found that the D/h affects the transmission coefficient very slightly. By comparing K_R and K_T with those of the isolated breakwater, it is found that the value of K_R can be reduced by the oscillating buoy, without affecting the value of K_T. For the CWR in Figure 5(c), the trend of bimodal curve can also be found

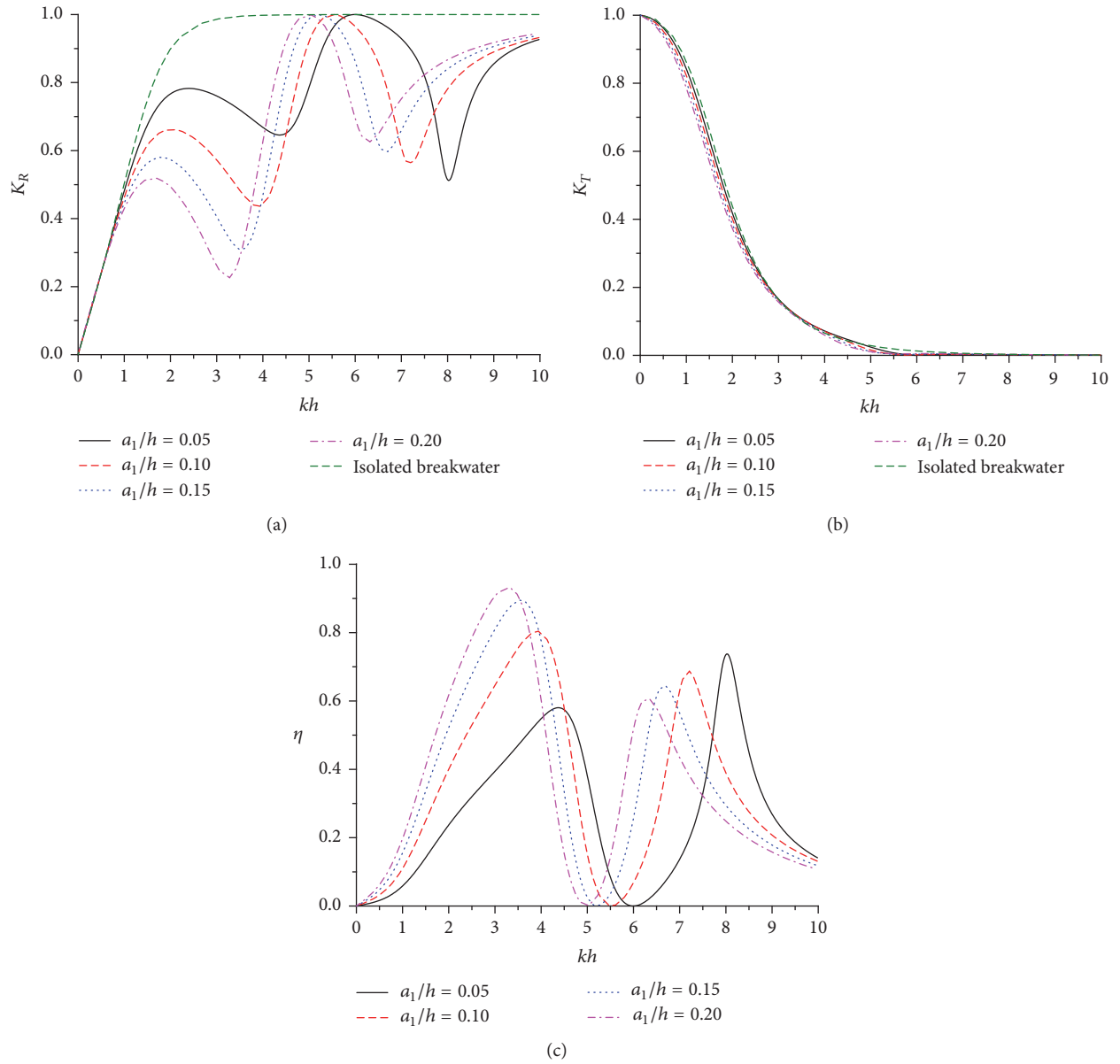

FIGURE 3: Variations of reflection coefficient K_R, transmission coefficient K_T, and CWR η versus the dimensionless wavenumber kh for cases with different structure breadths (a_1/h = 0.05, 0.1, 0.15, and 0.2).

in all these four cases. However, both peak values and their corresponding kh vary in different cases. The first peak from the lower frequency region decreases with D/h increasing, but it is opposite for the second peak. Both peaks shift to the lower frequency region as the spacing increases.

3.5. Effects of PTO Damping. The optimal damping corresponding to the isolated case is used to calculate CWR of the system in Sections 3.2–3.5. The influence of the PTO damping on the hydrodynamics of the system is considered in this subsection. The geometrical parameters of two structures are kept constant as $a_1/h = 0.2$, $a_2/h = 0.6$, $d_1/h = 0.1$, $d_2/h = 0.25$, and $D/h = 0.05$. Figure 6 shows variations of the reflection coefficient K_R, the transmission coefficient K_T, and the CWR η, with different PTO damping (i.e., $\lambda_{\text{PTO}} = 0.5\lambda_{\text{isolation}}$, $0.75\lambda_{\text{isolation}}$, $1\lambda_{\text{isolation}}$, $1.25\lambda_{\text{isolation}}$, and $1.5\lambda_{\text{isolation}}$).

Figures 6(a), 6(b), and 6(c) show the variations of reflection coefficient K_R, transmission coefficient K_T, and CWR η versus the dimensionless wavenumber kh, respectively, with different PTO damping. Variation trends of K_R versus kh, K_T versus kh, and η versus kh for different PTO damping are similar. For K_R versus kh in Figure 6(a), the peak value changed little and the trough value changes significantly, which mainly presents as the first trough value decreasing first and then increasing and the second trough value

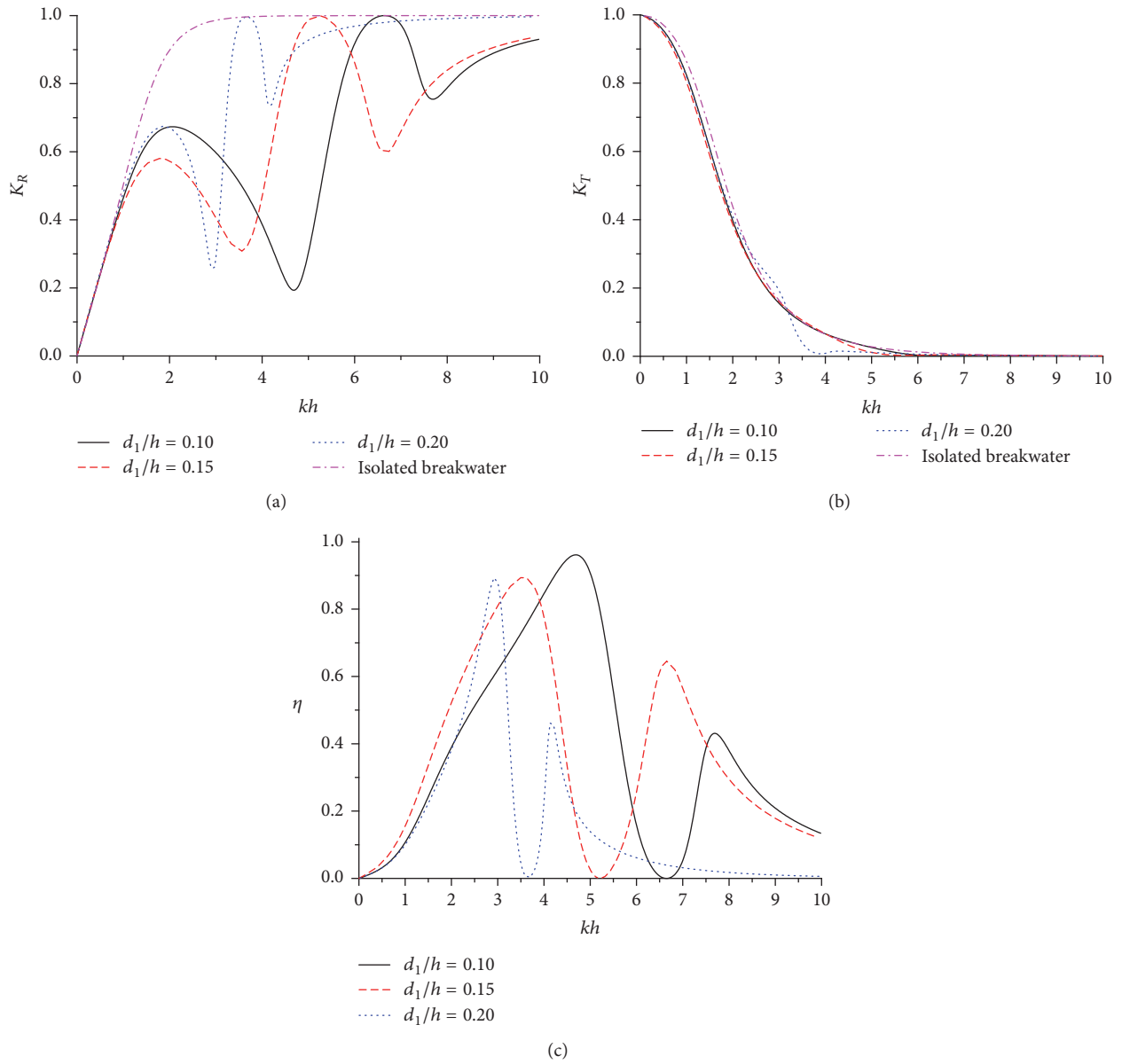

FIGURE 4: Variations of the reflection coefficient K_R, transmission coefficient K_T, and CWR η versus the dimensionless wavenumber kh for cases with different drafts of the front buoy ($d_1/h = 0.1$, 0.15, and 0.2).

increasing as the PTO damping increases. However, minor changes can be drawn from the variations of K_T versus kh in Figure 6(b). For the CWR, the first peak value increases and then approaches a stable value and the second peak value increases with the increasing of the PTO damping. The wavenumbers corresponding to the trough value of CWR are not sensitive to PTO damping.

3.6. Wave Exciting Force on the Breakwater. Since wave exciting force is the key element in design of the marine structures, the horizontal and the vertical wave exciting forces acting on the rear breakwater are of interest. Two scenarios are considered: (1) a case with the front buoy, that is, $a_1/h = 0.2$, $a_2/h = 0.6$, $d_1/h = 0.1$, $d_2/h = 0.25$, and $D/h = 0.05$ and (2) a case without the front buoy, that is, $a_1/h = 0.0$, $a_2/h = 0.6$, $d_1/h = 0.0$, and $d_2/h = 0.25$. Conveniently, we call the former one Case 1 and the latter Case 2. The horizontal force $F_{x,2}$ and vertical force $F_{z,2}$ are nondimensionalized by ρghA, symbolically, $F_{x,2}/\rho ghA$ and $F_{z,2}/\rho ghA$, respectively.

Figures 7(a) and 7(b) show the variations of $F_{x,2}/\rho ghA$ and $F_{z,2}/\rho ghA$ versus the dimensionless wavenumber kh, respectively. It can be seen that both $F_{x,2}/\rho ghA$ and $F_{z,2}/\rho ghA$ of Case 1 are obviously greater than that of Case 2 in the vicinity of $kh = 5.3$. That is to say, the existence of the front buoy may cause the sudden increase of the horizontal force and the vertical force at certain frequencies. This shall be paid

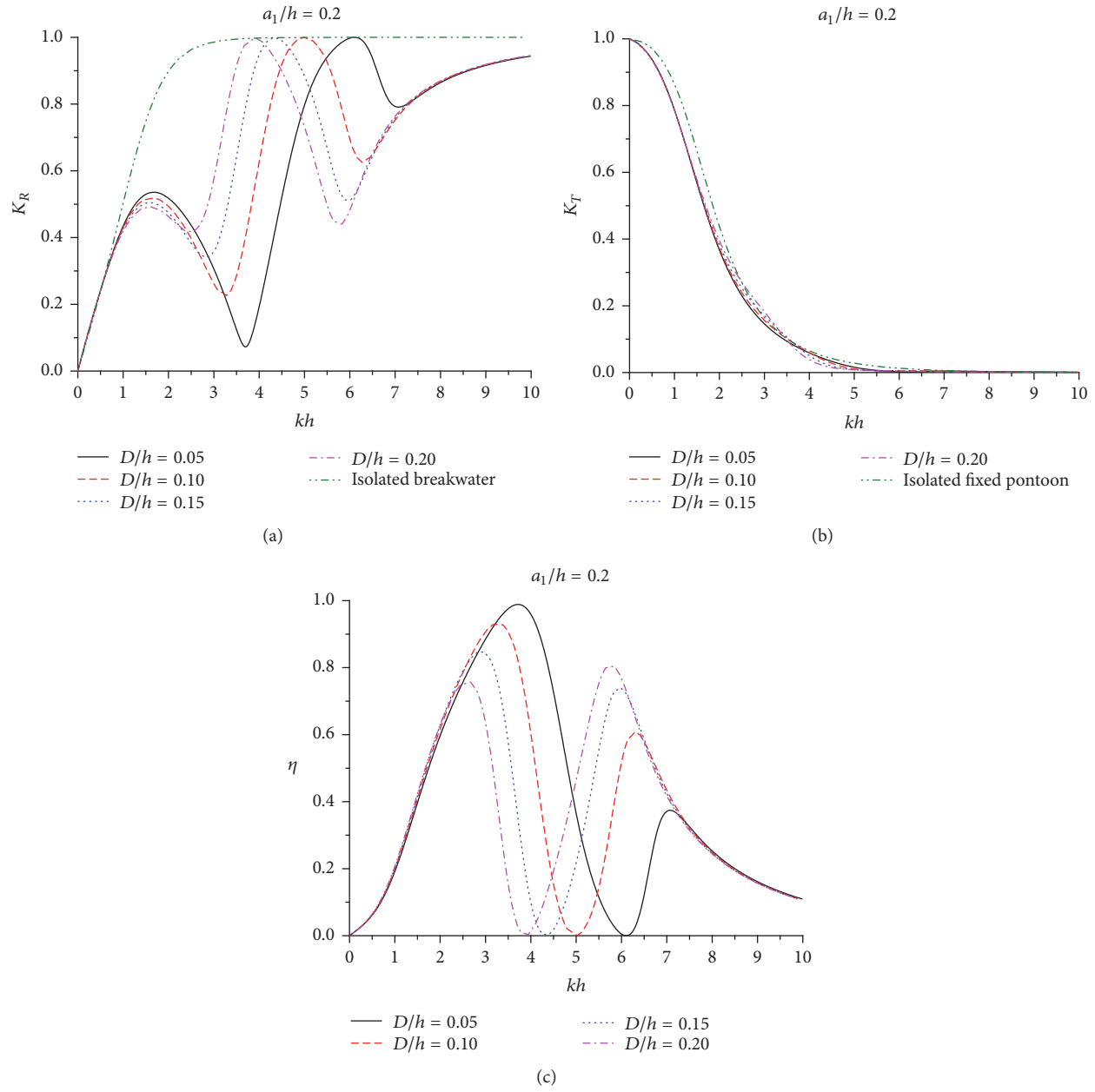

FIGURE 5: Variations of the reflection coefficient K_R, transmission coefficient K_T, and CWR η versus the dimensionless wavenumber kh for cases with different spacing (D/h = 0.05, 0.1, 0.15, and 0.2).

attention to while designing such a system from viewpoint of the safety.

4. Conclusions

Hydrodynamic performance of an oscillating buoy WEC installed in front of an existing fixed box-type breakwater was studied systematically with respect to the geometrical and PTO parameters, based on potential-flow theory. The present study reveals that the maximum efficiency of the energy extraction can be 80% or even higher. Compared with the isolated box-type breakwater, the reflection coefficient was reduced effectively by the integration of such an oscillating buoy WEC. However, the transmission coefficients were changed less for the same cases. The possibility of effectively capturing the wave energy by using the oscillating buoy WEC integrated into breakwaters was shown.

It should be noted that even though the wave reflection can be greatly reduced at a broad frequency range, there still exist certain frequencies at which the reflection coefficient is still large and the corresponding CWR is close to zero. The obvious increase of the wave exciting force on the

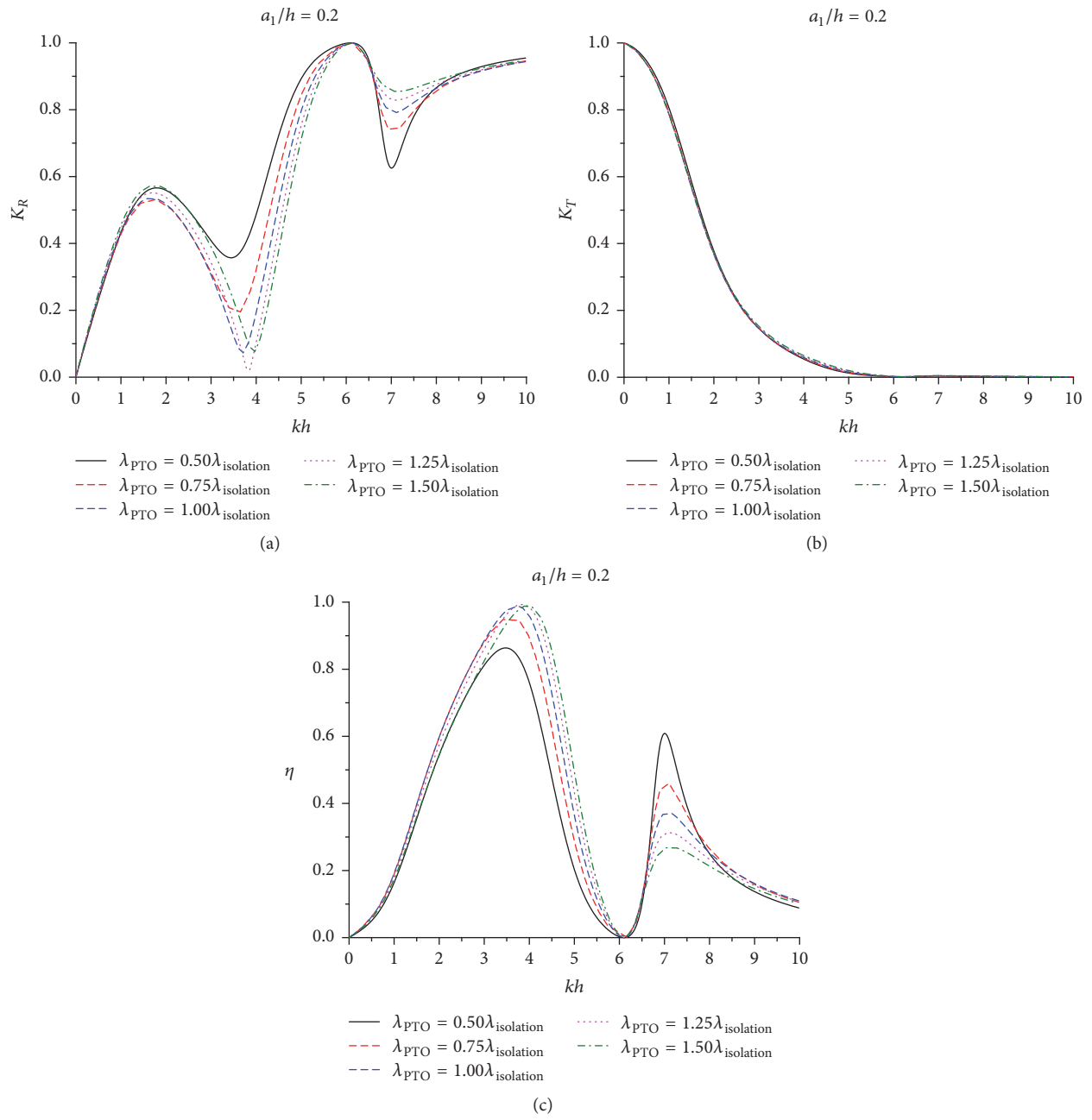

FIGURE 6: Variations of the reflection coefficient K_R, transmission coefficient K_T, and CWR η versus the dimensionless wavenumber kh for cases with different PTO damping ($\lambda_{PTO} = 0.5\lambda_{isolation}$, $0.75\lambda_{isolation}$, $1\lambda_{isolation}$, $1.25\lambda_{isolation}$, and $1.5\lambda_{isolation}$).

rear breakwater can be found at certain frequencies. In the practical applications, the buoy breadth and draft and the spacing between two structures should be optimized to make the high efficiency region located at the dominant wave frequency range and avoid the frequency range with peak wave loads. In addition, at this preliminary stage of the design, only the linear solution within potential-flow theory is discussed in this study. In the future, physical experiments will be further performed to investigate the viscous and nonlinear effects on the hydrodynamic performance of such WEC system.

Conflicts of Interest

The authors declare that there are no conflicts of interest regarding the publication of this paper.

Acknowledgments

The authors would like to acknowledge the financial support of the National Natural Science Foundation of China (Grants nos. 51379037 and 51679036) and the Royal Academy of Engineering under the UK-China Industry Academia Partnership

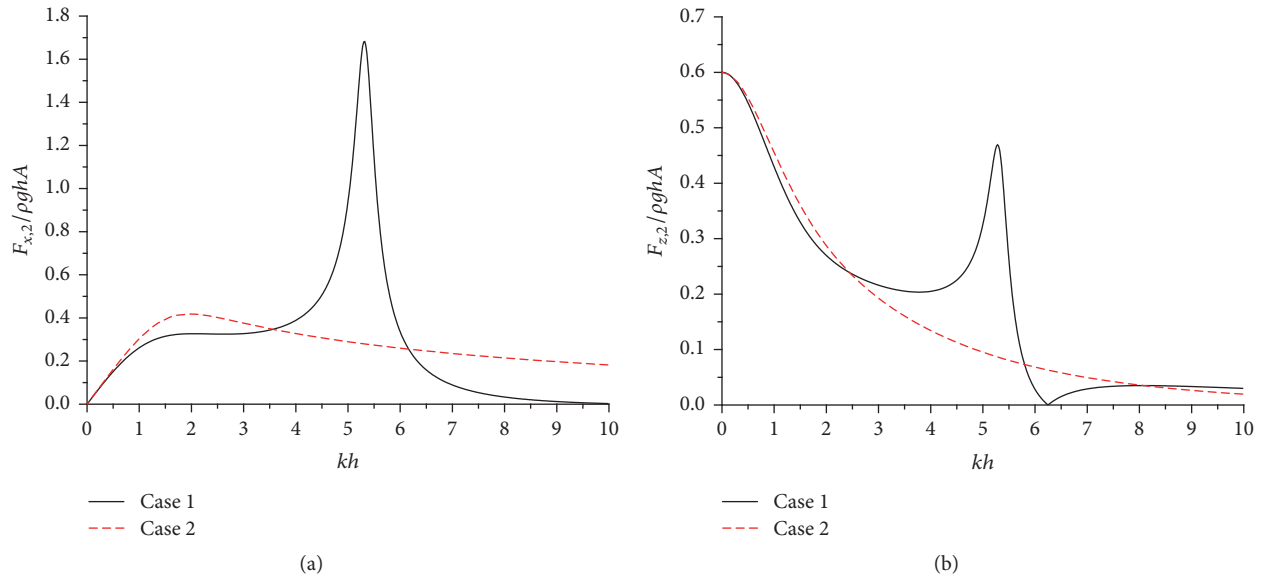

FIGURE 7: Variations of the dimensionless horizontal force $F_{x,2}/\rho ghA$ and dimensionless vertical force $F_{z,2}/\rho ghA$ versus the dimensionless wavenumber kh for Cases 1 and 2.

Programme (Grant no. UK-CIAPP\73). Thanks also are due to Dr. Si-Ming Zheng from Tsinghua University for valuable discussions.

References

[1] E. Koutandos, P. Prinos, and X. Gironella, "Floating breakwaters under regular and irregular wave forcing: Reflection and transmission characteristics," *Journal of Hydraulic Research*, vol. 43, no. 2, pp. 174–188, 2005.

[2] B. H. Adee, "A Review of developments and problems in using floating breakwaters," in *Proceedings of 8th Offshore Technology Conference*, pp. 225–236, Houston, Texas, USA, 1976.

[3] B. L. McCartney, "Floating breakwater design," *Journal of Waterway, Port, Coastal and Ocean Engineering*, vol. 111, no. 2, pp. 304–318, 1985.

[4] A. G. Abul-Azm and M. R. Gesraha, "Approximation to the hydrodynamics of floating pontoons under oblique waves," *Ocean Engineering*, vol. 27, no. 4, pp. 365–384, 2000.

[5] N. Drimer, Y. Agnon, and M. Stiassnie, "A simplified analytical model for a floating breakwater in water of finite depth," *Applied Ocean Research*, vol. 14, no. 1, pp. 33–41, 1992.

[6] Y. H. Zheng, Y. M. Shen, Y. G. You, B. J. Wu, and D. S. Jie, "Wave radiation by a floating rectangular structure in oblique seas," *Ocean Engineering*, vol. 33, no. 1, pp. 59–81, 2006.

[7] I. Diamantoulaki, D. C. Angelides, and G. D. Manolis, "Performance of pile-restrained flexible floating breakwaters," *Applied Ocean Research*, vol. 30, no. 4, pp. 243–255, 2008.

[8] J. Lee and W. Cho, "Effects of mean wave drift force on mooring tension and performance of a moored floating breakwater," *KSCE Journal of Civil Engineering*, vol. 6, no. 2, pp. 193–201, 2002.

[9] C. Michailides and D. C. Angelides, "Modeling of energy extraction and behavior of a Flexible Floating Breakwater," *Applied Ocean Research*, vol. 35, pp. 77–94, 2012.

[10] F. He and Z. Huang, "Hydrodynamic performance of pile-supported OWC-type structures as breakwaters: An experimental study," *Ocean Engineering*, vol. 88, pp. 618–626, 2014.

[11] B. Chen, D. Ning, C. Liu, C. A. Greated, and H. Kang, "Wave energy extraction by horizontal floating cylinders perpendicular to wave propagation," *Ocean Engineering*, vol. 121, pp. 112–122, 2016.

[12] F. He and Z. Huang, "Using an oscillating water column structure to reduce wave reflection from a vertical wall," *Journal of Waterway, Port, Coastal and Ocean Engineering*, vol. 142, no. 2, Article ID 04015021, 2016.

[13] D. Ning, X. Zhao, M. Göteman, and H. Kang, "Hydrodynamic performance of a pile-restrained WEC-type floating breakwater: An experimental study," *Renewable Energy*, vol. 95, pp. 531–541, 2016.

[14] S. Zheng and Y. Zhang, "Wave diffraction and radiation by multiple rectangular floaters," *Journal of Hydraulic Research*, vol. 54, no. 1, pp. 102–115, 2016.

[15] J. Falnes, *Ocean Waves and Oscillating Systems*, Cambridge University Press, UK, 2002.

[16] H. A. Wolgamot, R. Eatock Taylor, and P. H. Taylor, "Effects of second-order hydrodynamics on the efficiency of a wave energy array," *International Journal of Marine Energy*, vol. 15, 2016.

[17] X. Garnaud and C. C. Mei, "Bragg scattering and wave-power extraction by an array of small buoys," *Proceedings of the Royal Society A: Mathematical, Physical and Engineering Sciences*, vol. 466, no. 2113, pp. 79–106, 2010.